WILEY **NMR** IN BIOMEDICINE

RESEARCH ARTICLE

An extended vascular model for less biased estimation of permeability parameters in DCE-T1 images

Siamak P. Nejad-Davarani[1,2,3] [ID] | **Hassan Bagher-Ebadian[1,4]** | **James R. Ewing[3,4]** | **Douglas C. Noll[2]** | **Tom Mikkelsen[5]** | **Michael Chopp[3,4]** | **Quan Jiang[3,4]**

[1] Department of Radiation Oncology, Henry Ford Health System, Detroit, MI, USA

[2] Department of Biomedical Engineering, University of Michigan, Ann Arbor, MI, USA

[3] Department of Neurology, Henry Ford Health System, Detroit, MI, USA

[4] Department of Physics, Oakland University, Rochester, MI, USA

[5] Department of Neurosurgery, Henry Ford Health System, Detroit, MI, USA

Correspondence
Siamak P. Nejad-Davarani, Department of Radiation Oncology, Henry Ford Health System, Detroit, MI, USA.
Email: siamak@umich.edu

One of the key elements in dynamic contrast enhanced (DCE) image analysis is the arterial input function (AIF). Traditionally, in DCE studies a global AIF sampled from a major artery or vein is used to estimate the vascular permeability parameters; however, not addressing dispersion and delay of the AIF at the tissue level can lead to biased estimates of these parameters. To find less biased estimates of vascular permeability parameters, a vascular model of the cerebral vascular system is proposed that considers effects of dispersion of the AIF in the vessel branches, as well as extravasation of the contrast agent (CA) to the extravascular-extracellular space. Profiles of the CA concentration were simulated for different branching levels of the vascular structure, combined with the effects of vascular leakage. To estimate the permeability parameters, the extended model was applied to these simulated signals and also to DCE-T1 (dynamic contrast enhanced T_1) images of patients with glioblastoma multiforme tumors. The simulation study showed that, compared with the case of solving the pharmacokinetic equation with a global AIF, using the local AIF that is corrected by the vascular model can give less biased estimates of the permeability parameters (K^{trans}, v_p and K_b). Applying the extended model to signals sampled from different areas of the DCE-T1 image showed that it is able to explain the CA concentration profile in both the normal areas and the tumor area, where effects of vascular leakage exist. Differences in the values of the permeability parameters estimated in these images using the local and global AIFs followed the same trend as the simulation study. These results demonstrate that the vascular model can be a useful tool for obtaining more accurate estimation of parameters in DCE studies.

KEYWORDS

arterial input function, cerebral tumors, DCE-MRI, dynamic contrast enhanced imaging, vascular modeling, vascular permeability

1 | INTRODUCTION

One of the challenges in dynamic contrast enhanced (DCE) studies is estimation of the time trace of local plasma contrast agent (CA) concentration or the arterial input function (AIF) at the tissue level.

Abbreviations used: AIC, Akaike information criterion; AIF, arterial input function; ASL, arterial spin labeling; BVM, basic vascular model; CA, contrast agent; CBF, cerebral blood flow; DCE, dynamic contrast enhanced; DCE-CT, dynamic contrast enhanced computed tomography; DCE-MR, dynamic contrast enhanced magnetic resonance; DSC, dynamic susceptibility contrast; EES, extravascular-extracellular space; GBM, glioblastoma multiforme; k_b, inverse transfer rate constant; K^{trans}, vascular transfer rate constant; MTT, mean transit time; PET, positron emission tomography; SM, standard model; SPGRE, spoiled gradient echo; SSE, sum of squared errors; v_e, extravascular-extracellular space volume; v_p, vascular plasma volume

We previously introduced a vascular transfer function of the brain that could model delay and dispersion of the CA concentration profile at different levels of the vascular branching tree.[1] This transfer function is based on laws of fluid dynamics and vascular morphology. Previously, Gall et al[2] and Kellner et al[3] had used a similar approach and derived a vascular tree model to explain delay and dispersion of the arterial spin labeling (ASL) bolus;[4] they also used this model to estimate the residue function for brain tissue in perfusion measurements.[5] These models assume that there is no leakage of the CA to the extravascular-extracellular space (EES). We used this transfer function to derive a model and by applying it to dynamic contrast enhanced computed tomography (DCE-CT) images and using the estimated model parameters, created an arrival time map of the brain.

In the MRI field, dynamic susceptibility contrast (DSC) imaging is the method of choice for perfusion studies in which mean transit time (MTT), cerebral blood flow (CBF) and cerebral blood volume are estimated[6]; DSC is based on changes of the T_2^* signal in the dynamic images.[6] In dynamic contrast enhanced magnetic resonance imaging (DCE-MRI) studies, dynamic series of T_1-weighted images are acquired and are mainly used for estimation of vascular permeability parameters such as vascular transfer rate constant (K^{trans}), vascular plasma volume (v_p) and EES volume (v_e).[8–10] Estimation of the permeability parameters can be done using pharmacokinetic models and one of these which is widely used is the standard model (SM) or extended Tofts model.[11] One of the main components in this model is the AIF. Theoretically, this should be the local AIF that is sampled directly at the inlet to the tissue being studied; however, in practice usually the AIF sampled from a major artery is used,[12] which results in eliminating the effects of dispersion and delay of the AIF.[13] Inaccurate estimation of the AIF at the tissue level for use in permeability and perfusion analyses could substantially add bias to the estimated hemodynamic and permeability maps. Calamante et al used independent component analysis to show that delay and dispersion of the AIF can cause underestimation of the CBF and overestimation of the MTT in DSC studies.[14] In their study, they showed that, although the delay can be corrected using the information of the arrival time of the bolus in the tissue, correcting for the dispersion should be done using a vasculature model. Lee et al used a model of tissue microcirculation based on tracer kinetics and Bayesian probability theory to estimate the localized AIF in DSC images and used this to estimate perfusion parameters[15]; permeability parameters found by employing these local AIFs showed strong correlation with those measured by quantitative positron emission tomography with $H_2[^{15}O]$.

In the DCE-MR area, Fluckiger et al presented a method for blind estimation of the local AIF based on the alternating minimization with model (AMM) method[16]; to estimate the local AIF, they constrained it with a model containing three gamma-variate curves. Their results show that, compared with using the local AIF, the current method of using arterially measured AIFs biases the resulting parameters high, especially in regions where more dispersion of the AIF is expected. In one approach, to eliminate the need for direct AIF measurement, Yankeelov et al proposed a method for quantitative analysis of DCE-MRI by comparing the CA concentration profile of tissues of interest with that of a reference region. Using this method, K^{trans} and v_e were estimated but a validation of the final results was not performed.[17]

In this paper, to address the effects of extravasation, we extend our basic vascular model (BVM) that we previously introduced[1] by combining it with the SM. Next, by simulating the AIF at different levels of the vascular system and also adding effects of vascular leakage to the simulated CA concentration profiles, we compare the results of using our model-corrected local AIF for estimating the permeability parameters with the SM to those estimated using the global AIF. Finally we perform the same comparison using DCE-MR images of a patient with a cerebral tumor.

2 | MATERIALS AND METHODS

All modeling and calculations were done in MATLAB (Release 2010b, MathWorks, Natick, MA, USA).

2.1 | The basic vascular model

2.1.1 | Transfer function of the vascular pathway

We previously introduced a model to address dispersion and delay of the CA profile when flowing from a main artery down to the lower levels of the vascular tree in the brain.[1,18] This model is mainly based on a previously derived equation for describing the transfer function of a single vessel with laminar flow.[4,18] The transfer function is a function of t_{0n}, the time required for the fluid on the central axis of the tube to pass through the a vessel at the nth branching level:

$$h_n(t) = \begin{cases} 0 & t < t_{0n} \\ \dfrac{2t_0^2}{t^3} & t \geq t_{0n} \end{cases} \quad n = 1,\ 2, ..., 6 \qquad (1)$$

Where

$$t_{0n} = \frac{D_{0n}}{v_{0n}}. \qquad (2)$$

Here, D_{0n} is the length and v_{0n} the maximum velocity of blood in the vessel (or the velocity along the central axis) at the nth level. The interesting point about this transfer function is that it can describe each vessel segment based on only one parameter (t_{0n}). This parameter is not related to the injection time of the CA, and based on Equation 2 depends only on the blood velocity in the vessel and its length. We will refer to t_{0n} as the branch delay, which is a characteristic of each branch, assuming that blood flow is constant. We selected the maximum value of $n = 6$ based on the study done by Wright et al where they measured the number of arterial branching levels in the different brain regions using magnetic resonance angiography.[19]

Under certain assumptions, the delay time, t_{0n} of each segment in the vascular tree can be considered equal, and in this case the transfer function of all the sequential branches can be considered identical. In this case the parametric equation of the transfer function from the opening of a main branch to the end of one of the sub-branches at the nth level of the vascular tree can be expressed as

$$h(t)_{1\ t0\ n} = g \times [h(t)_1]^{*n} \qquad (3)$$

where "*n" denotes n repeated convolutions. Here g is a gain factor compensating for the fractional volume of the vessels in the tissue.

By sampling the CA profile from a voxel in the DCE image series, and also by sampling the AIF in a voxel representing the circle of Willis, we can write the following equation:

$$AIF_L(t) = h(t)_{1\ t0\ n} * AIF(t). \qquad (4)$$

$AIF_L(t)$ is the local AIF in the tissue. If the vessels are intact and do not have CA leakage, the CA profile sampled from a voxel in the DCE images can represent $AIF_L(t)$. It should be noted that in this equation, the effects of the capillaries on dispersing the AIF have not been considered. To find the transfer function that can best describe the relation between the AIF and $AIF_L(t)$ for each voxel in the image, we developed a procedure based on the Nelder–Mead simplex search method of Lagarias et al[20] as a non-linear fitting method with the

sum of squared errors (SSE) as the cost function, along with the Akaike information criterion (AIC),[21] to find the best configuration of the transfer function (based on the number of branching layers, n) that can transform the AIF to $AIF_L(t)$. Since initially it is not known to which branching level of the vascular tree the selected voxel belongs, the fitting procedure is repeated separately for six configurations of one to six layers of branching, to find the following set of parameters for the transfer function for each configuration:

$$[g, t_{01}]. \tag{5}$$

After finding the best fit transfer function for each configuration of the vascular tree, using the fitting residual values, the best model is selected using the AIC to represent the transfer function that transfers the AIF to the selected $AIF_L(t)$.

The model described above (basic vascular model or BVM) has been designed to explain dispersion and delay of the AIF in the vascular tree with no extravasation in any of the vessels. As we will explain in the following sections, the model in its current form will not be able to explain the profile of the CA concentration when the signal is sampled from areas with leaky vessels.

2.2 | Extending the basic vascular model

When the tissue concentration signal is sampled from voxels in image areas containing vessels with no leakage, the signal mainly represents the CA concentration profile in the intravascular space. This profile is generally a dispersed form of the AIF in major vessels; however, when the CA leaks into the extravascular space, the sampled tissue concentration signal will follow a different trend. Based on this observation, to address the changes of the CA profile in areas with leaky vasculature and to find a more accurate estimation of the intravascular (plasma) CA concentration profile in these vessels, we modified the BVM to include effects of leakage of the CA to the extravascular space.

2.2.1 | Adding permeability parameters to the basic vascular model

One of the models describing tracer kinetics is the extended Tofts Model or SM. According to the SM, which is a two compartmental model,[13,22] the relationship between $C_t(t)$ (tissue concentration profile of the CA) and $C_p(t)$ (plasma concentration profile of the CA) can be described as follows:

$$C_t(t) = K^{trans} \int_0^t e^{-k_b(t-\tau)} C_p(\tau) d\tau + v_p C_p(t). \tag{6}$$

In this equation, the tissue concentration of CA, $C_t(t)$, is composed of two main components: The first term on the right, $K^{trans} \int_0^t e^{-k_b(t-\tau)} C_p(\tau) d\tau$ represents the component of the signal that is due to leakage of the CA to the extravascular space and is dependent on the forward (K^{trans}) and inverse (k_b) transfer rate constants. The second term, $v_p C_p(t)$, basically represents the time trace of the plasma CA concentration in the vessels that feed the tissue from which $C_t(t)$ is being sampled. Depending on the type of vasculature leakage, some of the permeability parameters may not be taken into account and

Equation 6 may follow different models of vascular extravasation as described below.[10,23]

I. Impermeable vasculature where the blood–brain barrier is intact ($K^{trans} = 0$, $k_b = 0$, $v_p \neq 0$).

II. Moderate influx, which is observed as leakage without efflux ($K^{trans} \neq 0$, $k_b = 0$, $v_p \neq 0$).

III. Fast leakage, which leads to bidirectional exchange ($K^{trans} \neq 0$, $k_b \neq 0$, $v_p \neq 0$).

Figure 1 shows a schematic diagram of the signal components of the extended Tofts model and their relation. $AIF(t)$ is the CA profile sampled at the location of one of the major arteries. The cube in this figure represents an imaginary voxel in the image from which the tissue CA concentration profile, $C_t(t)$, is being sampled. $C_p(t)$ is the plasma CA concentration in the vessel (or vessels) feeding the tissue in the voxel.

As we noted in the introduction section, in conventional methods of calculating the permeability parameters using the pharmacokinetic model, for the profile of $C_p(t)$, the CA profile sampled from one of the major arteries (in the image) or even veins (such as the superior sagittal sinus) is usually used; however, this is not representative of the CA profile in tissue since it does not address dispersion of the CA profile at different levels of the vascular tree and can lead to biased estimates of the permeability parameters. In image areas with non-leaky vessels, the sampled profile basically represents only the intravascular CA concentration which can be described with the BVM. To find an equation for describing the intravascular CA concentration profile in leaky vessels, we added a new feature to the vascular transfer function that we defined by Equation 3. If in Equation 6 we replace the plasma CA concentration profile, $C_p(t)$, with the local interpretation of the AIF in tissue, the pharmacokinetic model can be written as

$$\begin{aligned} C_t(t) &= \frac{K^{trans}}{v_p} \int_0^t e^{-k_b(t-\tau)} AIF_L(\tau) d\tau + AIF_L(t) \\ &= \frac{K^{trans}}{v_p} \left(e^{-k_b t} * AIF_L(t) \right) + AIF_L(t). \end{aligned} \tag{7}$$
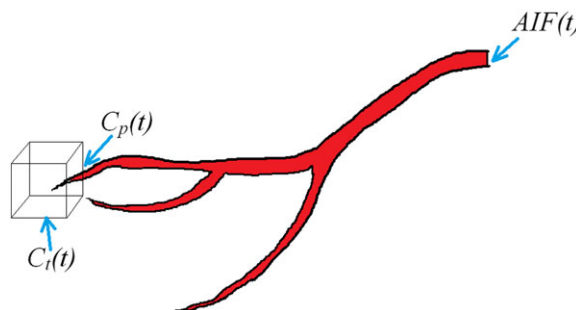

FIGURE 1 Schematic diagram showing the main components of the pharmacokinetic model and their location. $AIF(t)$ is the CA profile sampled at the location of one of the major arteries. The cube in this figure represents an imaginary voxel in the image from which the tissue CA concentration profile, $C_t(t)$, is being sampled. $C_p(t)$ is assumed to be the plasma CA concentration in the vessel (or vessels) feeding the tissue in the voxel

By replacing $AIF_L(t)$ from Equation 4 we have

$$C_t(t) = \frac{K^{trans}}{v_p}\left(e^{-k_b t} * AIF(t) * h(t)_{1\ t0\ n}\right) + AIF(t) * h(t)_{1\ t0\ n} \quad (8)$$

Or

$$C_t(t) = AIF(t) * \left[h(t)_{1\ t0\ n} * \left(\frac{K^{trans}}{v_p}e^{-k_b t} + \delta(t)\right)\right] = AIF(t) * h_E(t) \quad (9)$$

Where

$$h_E(t) = h(t)_{1\ t0\ n} * \left(\frac{K^{trans}}{v_p}e^{-k_b t} + \delta(t)\right). \quad (10)$$

The transfer function, $h_E(t)$, describes transformation of the AIF profile to the measured tissue concentration signal at different locations of the vascular structure, with or without leakage of the vessels. In the case where the vessels are intact (non-leaky), K^{trans} will be zero and the measured signal will be basically the intravascular plasma concentration of the CA in the tissue, which can be described by convolving the AIF with $h(t)_{1\ t0\ n}$. In the case where the vessels are leaky, $C_t(t)$ is the superposition of the intravascular and extravascular components of the signal, which are the two main components of this equation.

To find the best function that transfers the AIF to the tissue concentration signal, in addition to the six configurations of the vascular tree (as in the BVM), three configurations of the SM[10,23] (Models I, II and III) are also considered. Therefore for each signal, 18 different combinations of the transfer function are studied, and using the fitting residues for each, the best transfer function describing transformation of the AIF to the tissue CA concentration profile is selected using the AIC. After finding the curve that best fits to the sampled signal, using the parameters found in the fitting procedure and also the two main components of this transfer function, the transfer functions describing the extravascular and intravascular components of the tissue concentration signal can be constructed and by convolving them with the AIF profile, each can be described as:

$$C_t^I(t) = AIF(t) * h(t)_{est} \quad (11)$$

$$C_t^E(t) = \frac{K^{trans}}{v_p}e^{-k_b t} * AIF(t) * h(t)_{est}. \quad (12)$$

Here $C_t^I(t)$ and $C_t^E(t)$ are the intravascular and extravascular components of the tissue CA concentration profile and $h(t)_{est}$ is the estimated vascular transfer function.

2.3 | Subjects

Three treatment naïve patients with glioblastoma multiforme (GBM) were scanned using the procedure described below. The study was approved by the Henry Ford Health System Institutional Review Board and written informed consent was obtained from all subjects.

2.4 | DCE-MR image acquisition

DCE-MR image acquisition was performed on a 3 T GE Excite HD MR system (GE Healthcare, Waukesha, WI, USA) using a standard eight-channel phased-array RF coil. Before CA administration, T_1 mapping was obtained using DESPOT1 (driven equilibrium single pulse observation of T_1),[24] with T_E/T_R = 0.84/5.8 ms, 256 × 256 matrix size, 240 mm FOV, 16 slices with 5 mm thickness and six flip angles of 2°, 5°, 10°, 15°, 20° and 25°. These images were used to create the pre-contrast T_1 maps that were used as the baseline values for the 3D spoiled gradient echo (SPGRE) DCE-T1 procedure.[10] The 3D SPGRE DCE-T1 sequence included 70 image volumes acquired 5.9 s apart, all with a 20° flip angle, T_E/T_R = 0.84/5.8 ms, 256 × 256 matrix size, 240 mm FOV, 16 slices with 5 mm thickness. Total data acquisition was 6.8 min. CA (Magnevist; Bayer Healthcare Pharmaceuticals, Wayne, NJ, USA) was administered intravenously by power injection 20 s after the start of the DCE-T1 sequence, at a dose of 0.1 mmol/kg with a rate of 4 mL/s.

It has been shown that changes in the relaxivity (ΔR_1) are linearly related to CA concentration in tissue[25,26]; we previously derived an equation for extracting ΔR_1 signals from T_1-weighted SPGRE MRI data.[9] If T_E is selected such that $T_E \ll T_2^*$, the effects of T_2^* on ΔR_1 calculated from the SPGRE DCE-T1 data can be minimized,[10] which is the condition we had for acquiring our DCE-T1 images. By applying this equation to our DCE-T1 data we produced the ΔR_1 maps for this image sequence. The voxelwise ΔR_1 signals in these images were used for estimation of the permeability parameters with the SM. To adjust the equations for DCE-MR applications, we replace $C_t(t)$ with $(1 - Hct)\,\Delta R_{1t}(t)$ and AIF(t) with $\Delta R_{1a}(t)$ in Equation 9:

$$(1-Hct)\Delta R_{1t}(t) = \Delta R_{1a}(t) * h_E(t). \quad (13)$$

2.5 | Comparison of performance of the BVM and the extended model in normal and leaky vessels

To compare the performance of the BVM with its extended form for describing the CA concentration profile in brain areas with leaky or non-leaky vessels, we studied the tissue CA concentration signals sampled from two regions of the brain in a patient with GBM: one from the normal tissue and the other from the tumor area. For each model, based on the procedure explained in the methods section, we separately used the BVM and the extended model to find the best transfer function describing the transformation of the AIF to the CA concentration profile in each of these regions.

2.6 | Applying the extended model to DCE-T1 images for estimation of the permeability parameters

When using the extended model for estimation of the transfer function, for each voxel in the image, in addition to the parameters that describe the vascular structure connecting the major artery and the vessels passing through this voxel, the permeability parameters can also directly be estimated as a byproduct of the method. Depending on the model of leakiness that is being considered, at each branching

level, the transfer function can have one (v_p), two (v_p, K^{trans}) or three (v_p, K^{trans}, K_b) parameters to represent one of the three configurations of the SM. After estimating all 18 transfer functions based on the fitting procedure and selecting the best fit model, the permeability parameters can be estimated using the parameters of this model.

We previously reported another method that we had established for estimating permeability parameters[10] in DCE-T1 images. This method was also based on finding the best set of permeability parameters describing the three configurations of the SM. In this method, initially for each configuration, the best set of parameters that related the global AIF to the tissue CA concentration in each voxel was estimated using the simplex method. Next, using the F-test,[27] the best configuration was selected and the parameters satisfying this configuration of the SM were selected as the permeability parameters for this voxel. The difference between this method and using the extended model is basically using the global AIF versus the local AIF to solve the SM or Tofts equation. To compare the results, and to evaluate the results of employing the local AIF to estimate permeability parameters, we estimated the permeability parameter maps from the DCE-T1 images of the brain of a patient with GBM, using both methods.

2.7 | Simulation study

One of our main goals for developing the vascular model is to estimate the permeability parameters more accurately. We hypothesized that by employing the local AIF and using this to solve the pharmacokinetic model we will be able to find more accurate estimates of the permeability parameters. To test this hypothesis, we simulated the three models of vascular leakage at different branching levels of the vessels and compared the estimated values of the permeability parameters when using the global AIF versus the local AIF found by the vascular model. Our assumption was that the artery or arteriole that feeds the capillary bed can be from any of the six branching levels. Although this is not necessarily true, we did this to make our simulation more robust.

In the first step, using the AIF sampled from the circle of Willis in the ΔR_1 image series estimated from the DCE-MRI series of a human subject (with image acquisition parameters described in the previous section), we simulated curves of the dispersed AIF at six levels of the vascular system using our vascular model with values close to those in the arteries of the human brain. This provided the dispersed and delayed CA concentration profile at each of these layers. For Model I, which is considered to be the model with no vascular leakage, the only parameter that we accounted for was the fractional plasma volume, v_p. Using four different values of v_p (0.01, 0.02, 0.04 and 0.1), tissue concentration signals were simulated at each level of the vascular branching structure. To simulate the signals for Model II, the forward transfer rate constant (K^{trans}) was added to the equation to simulate leakage of the vessels. We did the simulation for a fixed value of the fractional plasma volume (v_p = 0.01) and two values of the forward transvascular transfer rate (K^{trans} = 0.001/min and 0.005/min). Finally, the tissue concentration signal was simulated using Model III of the pharmacokinetic model in which a third parameter, K_b, was added. Similar to the other two models, we estimated these three parameters using the two methods and compared the results. The simulation was done using K^{trans} = 0.005 and v_p = 0.01 and two values for K_b (0.2 and 0.5).

3 | RESULTS

3.1 | Applying the BVM to MRI data

Figure 2A shows one slice of a DCE-T1 image from a patient with GBM after injection of the CA. Figure 2B shows the CA concentration profile ($\Delta R_1(t)$) sampled from the voxels in the circle of Willis (as marked in Figure 2A) and Figure 2C shows the CA profile from an ROI sampled from the normal white matter area. Using the procedure explained in the methods section, we found the best transfer function (based on the BVM) explaining the transformation of the AIF to this local AIF. By convolving the AIF in Figure 2B with this transfer function, the bold curve in Figure 2E is estimated. To explore the performance of this model in other areas of the brain, we sampled a signal from an ROI in the tumor area as seen in Figure 1A. The CA concentration profile sampled from this ROI can be seen in Figure 2D. The tail of this profile does not follow the trend that is seen in the CA profile in the normal area. After applying the method above to this signal and finding the best fit, the bold curve in Figure 2F is estimated. As seen here, the BVM can only describe changes in the CA profile in intact vessels with no leakage, and in cases where leakage vascular exists it does not perform correctly

3.2 | Applying the extended model to MRI data

To test the extended model, we applied it to the CA concentration profile sampled from the tumor area (Figure 2A). The bold curve in Figure 3B shows the tissue CA concentration profile that was reconstructed by convolving the best selected transfer function with the AIF. As seen in this figure, this profile matches the original data very well. We applied the extended model to the CA profile sampled from the normal tissue and repeated the same procedure on it. Figure 3A shows the reconstructed profile. This profile is the same as the profile found using the BVM. Using the estimated parameters of the transfer function, the tissue concentration profile was decomposed into the intravascular and extravascular components. These can be seen in Figure 3C,D. When the signal is sampled from the normal tissue, the extravascular component appears to be non-existent and is seen as a flat line. However, for the signal sampled from the tumor area, these two components are separated as two different profiles: the intravascular signal and the extravascular signal, representing leakage of the CA to the EES.

We applied both models to all voxels in a slice of the DCE-T1 image series of the same patient. Figure 4 shows residual maps from the fitting procedure using the two models for different levels of the vascular tree. The residual values in the tumor area are much lower for the extended model, which means that this model can explain the trend of the CA profile in the leaky vasculature areas much better than the BVM. Finding the best fit in the lower levels may be due to the tumor being fed through a major artery in the lower branching levels.

3.3 | Estimation of permeability parameters in DCE-MR imaging using the extended model

Figure 5A, C and E shows the three permeability maps (v_p, K^{trans}, K_b) that were estimated by solving the pharmacokinetic model using the global AIF for the DCE-MR series of the slice shown in Figure 5G. Figure 5B,D,F shows the same maps estimated using the local AIF found by the extended model. As seen in the v_p map, in the non-leaky areas the values found by the two methods are very close; however, the v_p values in Figure 5A show lower values in the tumor area compared with Figure 5B. This can be interpreted as an underestimation of the plasma volume fraction in leaky areas when the global AIF is used. The outcome of the simulation study described in the next section confirms these results. Comparison of the corresponding K^{trans} and K_b maps when the extended model is used show that the values of K^{trans} and K_b when using the global AIF are both underestimated.
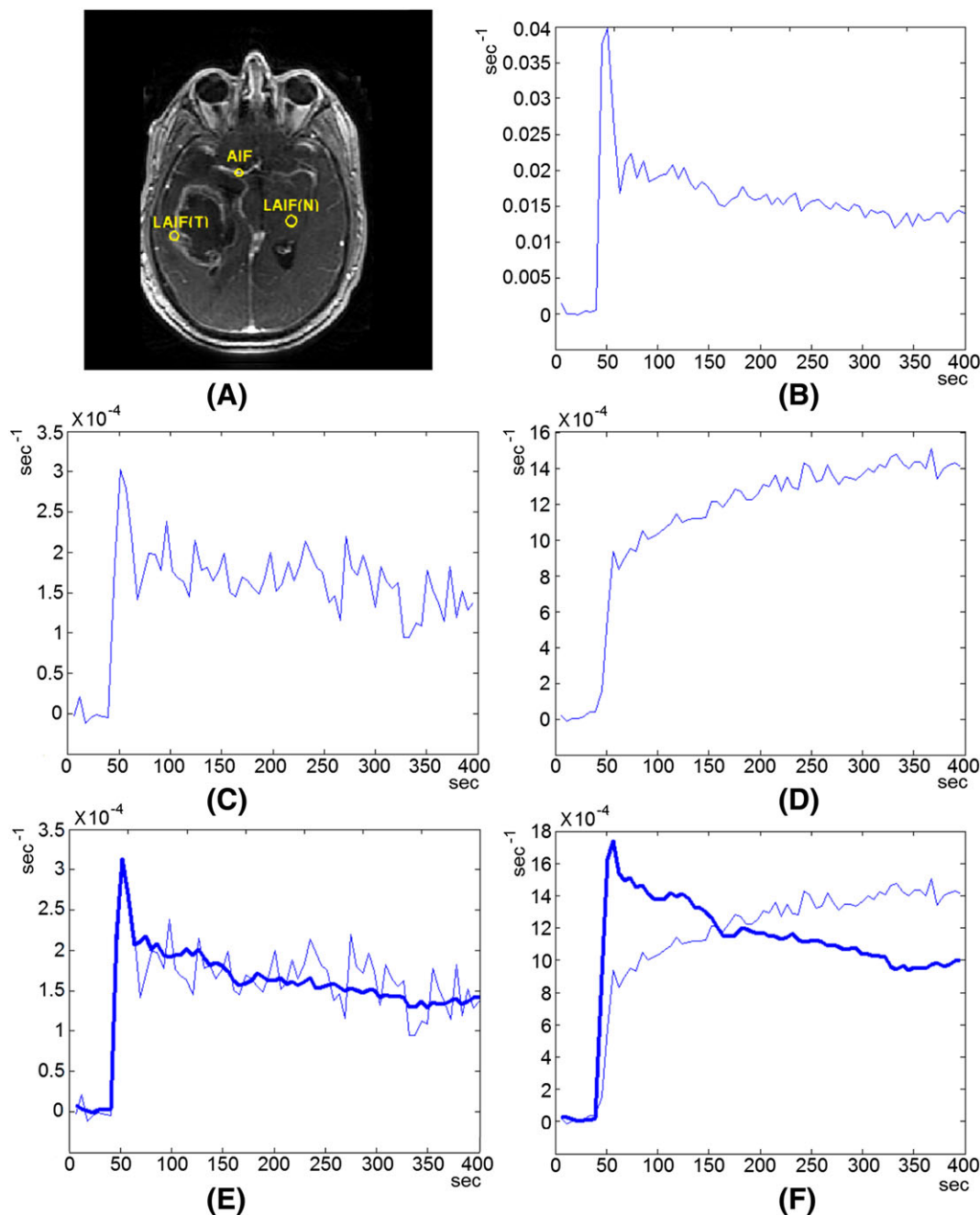

FIGURE 2 A, One slice of a post-contrast-injection DCE-MRI image from a patient with GBM with three ROIs from a major artery (AIF), normal tissue (LAIF(N)) and the tumor area (LAIF(T)). B-D, The CA profile sampled from the major artery (B) normal tissue (C, non-leaky vasculature) and the tumor area (D, leaky vasculature) from the DCE-MR image series. E,F, Using our vascular model, the transfer function that gave the best fit for each of the two CA profiles and the resulting local AIF was found. As seen here, in the case of non-leaky vasculature, after reconstruction using the best fit transfer function, the resulting local AIF can give a good estimation of the signal sampled from the tissue (E). However, in the case of the signal sampled from the tumor area (F), the best fit signal cannot follow the trend of the AIF and the best fit model is erroneously selected as the sixth level to minimize the residual error of the fitting procedure. The sum of squared errors (SSEs) for the fitted curves in E and F are 4.86×10^{-8} and 9.29×10^{-6} respectively
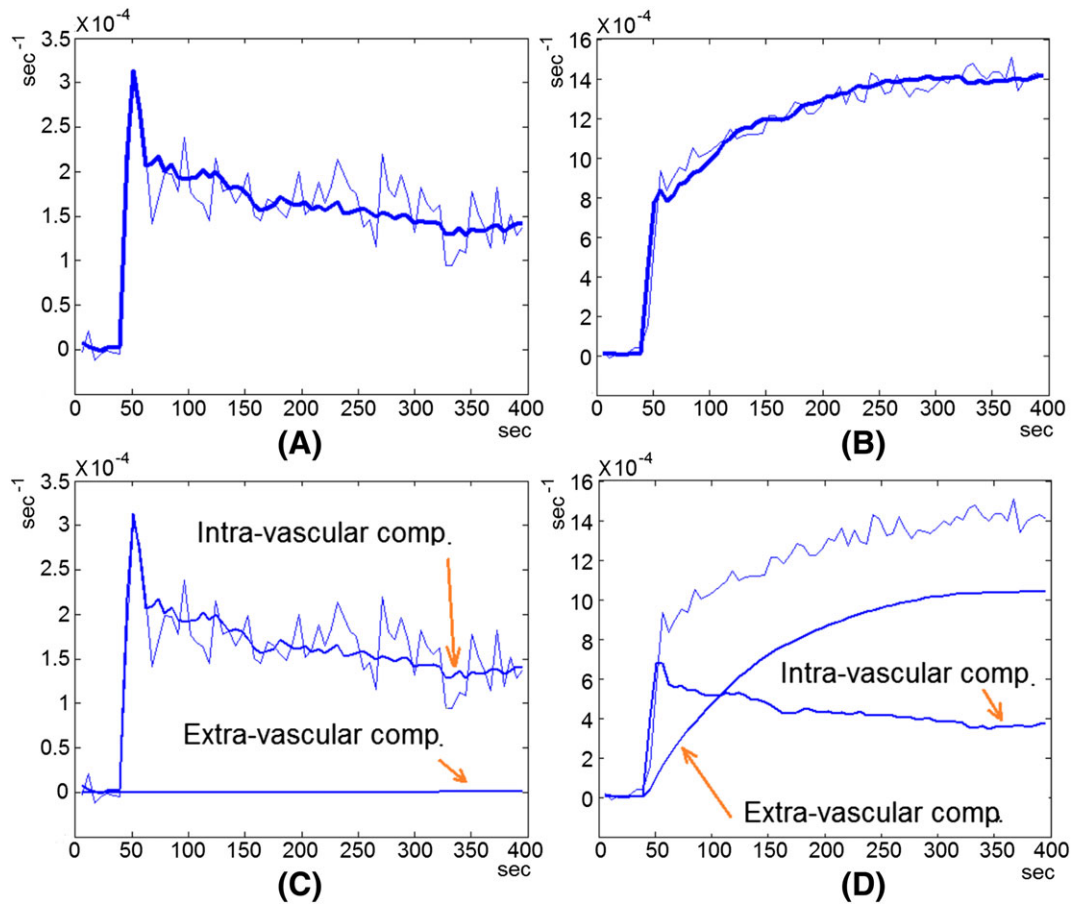
FIGURE 3 A,B, The profiles representing the tissue CA concentration (thin line) and the reconstructed profile after fitting and model selection (bold line) from the normal tissue (A) and the tumor area (B) as described in Figure 2. C,D, Intravascular and extravascular components of the reconstructed tissue concentration profiles, based on the decomposition using the extended vascular model. As seen here, in the case where the signal is sampled from the normal tissue (C), the extravascular component is a flat line, indicating no leakage to the extravascular space. However, when the signal is sampled from the tumor (D) the intravascular and extravascular components are separated, which may indicate the flow or extravasation properties of the vessels in the sampled region independently. The SSEs for the fitted curves in A and B are 4.86×10^{-8} and 2.98×10^{-7} respectively
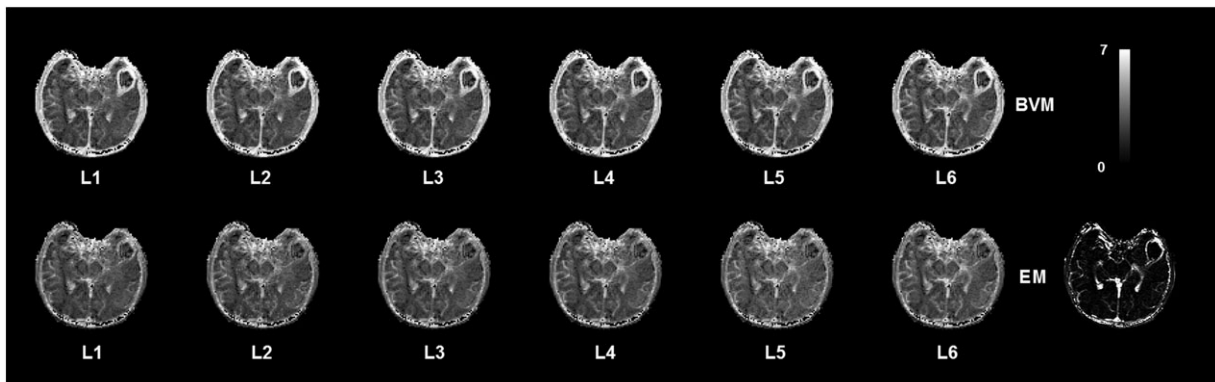

FIGURE 4 Maps of the fitting residual values using the BVM and the extended model in a set of DCE-MR images. Every voxel in each map represents the residue of the best fit function at each branching level of the vascular structure. For better representation of these maps, they have been scaled to $\log(10^8\ SSE)$. In areas of the brain outside the tumor, the residual values are almost identical for the EVM and BVM at each branching level, which indicates that the EVM can explain dispersion and delay of the AIF in non-leaky vessels similarly to the BVM. As seen here, the residual values in the tumor area are much lower for the EVM, which means that this model can explain the trend of the CA profile in the leaky vasculature areas much better than the BVM. Finding the best fit for the tumor at the fourth level may be due to the tumor being fed through a vessel at the fourth branching level

The total time for processing one slice of the DCE-MR images was approximately 3 h on an Intel Core i7, 2.70 GHz processor. This included 18 repetitions of the transfer function fitting algorithm for each voxel and finally selecting the best fit transfer function.

3.4 | Simulation study

In Figure 6 the results of estimating v_p using the two methods are presented. The signals were simulated for four values of v_p (0.01, 0.02, 0.04 and 0.1). The observation in all these graphs is that when the global AIF is used, starting from the first level of vascular branching, the value of v_p is underestimated, and the gap between the estimated

value and the nominal value increases as the tissue concentration signal gets more dispersed. However, the values estimated by the model corrected local AIF remain very close to the nominal value at all levels of vascular branching.

The plots in Figure 7 show the estimated values of K^{trans} and v_p in the case of simulating Model II, calculated using the global AIF and the model corrected local AIF, assuming that they are sampled from six different levels of the vascular tree. Figure 7A,B show the case where $v_p = 0.01$ and $K^{trans} = 0.001$/min and Figure 7C,D represents $v_p = 0.01$ and $K^{trans} = 0.005$/min. As seen here, in both configurations, the K^{trans} values found using the global AIF are overestimated at all branching levels, and as the vascular levels increase this value increases as well.
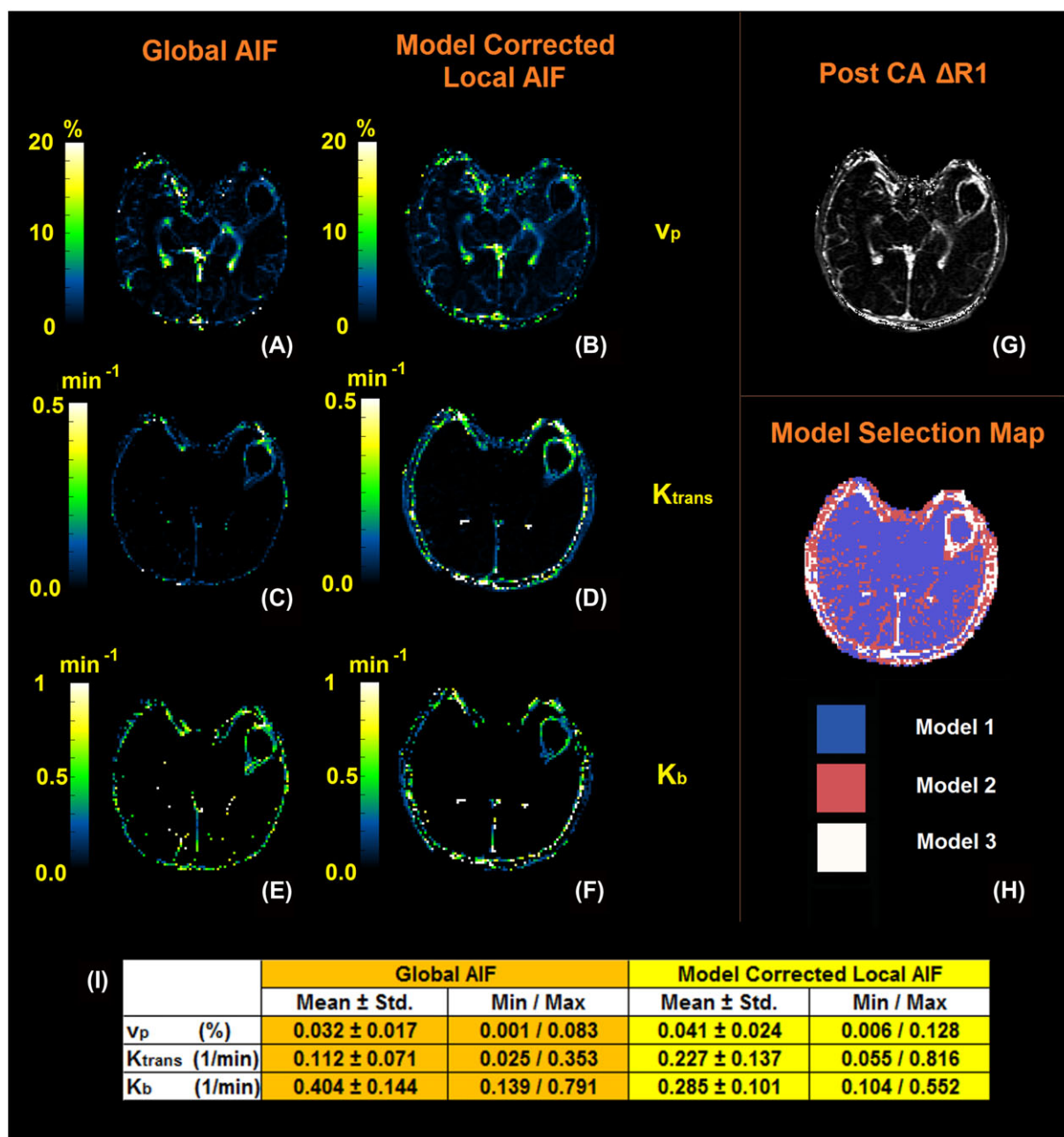

		Global AIF		Model Corrected Local AIF	
		Mean ± Std.	Min / Max	Mean ± Std.	Min / Max
Vp	(%)	0.032 ± 0.017	0.001 / 0.083	0.041 ± 0.024	0.006 / 0.128
Ktrans	(1/min)	0.112 ± 0.071	0.025 / 0.353	0.227 ± 0.137	0.055 / 0.816
Kb	(1/min)	0.404 ± 0.144	0.139 / 0.791	0.285 ± 0.101	0.104 / 0.552

FIGURE 5 A,C,E, The three permeability maps (v_p, K^{trans}, K_b) estimated by solving the pharmacokinetic model using the global AIF for the DCE-MR series of the slice shown in G. B,D,F Permeability maps estimated using the local AIF found by the vascular model. H, Model selection map estimated using the residual sum of squares from the fitting procedure and finding the minimum AIC. I, The mean, standard deviation, minimum and maximum values of v_p, K^{trans} and K_b measured in the voxels representing the tumor

In the case of the estimated v_p (similar to the case of the first configuration of the pharmacokinetic model), when using the global AIF, the fractional plasma volume is underestimated starting from the first level and is underestimated by about 80% of the nominal value when it reaches the last level. In the case of using the extended model the estimated value of v_p is always accurate.

The graphs comparing the estimated values of K^{trans}, K_b and v_p, using the two AIFs for two sets of Model III simulated signals, are plotted in Figure 8. As seen in both signal sets, the values of v_p, K^{trans} and K_b estimated using the local AIF are the same as the nominal values. Using the global AIF, the value of K^{trans} may be overestimated as much as 20-fold and K_b as high as six times the nominal value.

4 | DISCUSSION AND CONCLUSION

We introduced a model of the brain vascular system that explains dispersion and delay of the AIF at different levels of the vascular structure, combined with the effects of extravasation of the CA to the extravascular space. This model is an extension of a previous model of the vessels (BVM), which did not include effects of extravasation. The results of applying these models to DCE-T1 images of patients with GBM show that the extended vascular model is able to explain the CA concentration profile at different levels of the vascular tree in

areas of the brain, with or without leakage of the vessels. Moreover, simulation results showed that when solving the Tofts equation, if the local AIF provided by the vascular model is used instead of the global AIF, permeability parameters can be estimated more accurately.

The advantage of using the vascular model for solving the pharmacokinetic model as described by the Tofts equation is that it can provide an estimate the local AIF found in each voxel, which can lead to more accurate estimation of the permeability parameters. One by-product of using this model is that it can be used to decompose the tissue concentration signal of the CA into the intra- and extravascular components, which are basically the flow and leakage components of the signal. Extracting the extravascular component of the signal can lead to estimation of the permeability parameters with fewer data points and using shorter scan times. Overall, this model has the potential to address many open problems in DCE-MRI and DSC-MRI and also in DCE-CT applications, where this model can be used for simultaneous measurement of permeability and perfusion parameters. It should be noted that, although this model in its current form gives a reasonable estimate of the local AIF, a more complete model should take into account the effects of the capillaries on the dispersion, which can be added in future studies. However, the model in its current form is a big step forward towards finding less biased estimates of the permeability parameters. Another point is that in our model we selected the maximum number of branching levels as six levels; although there
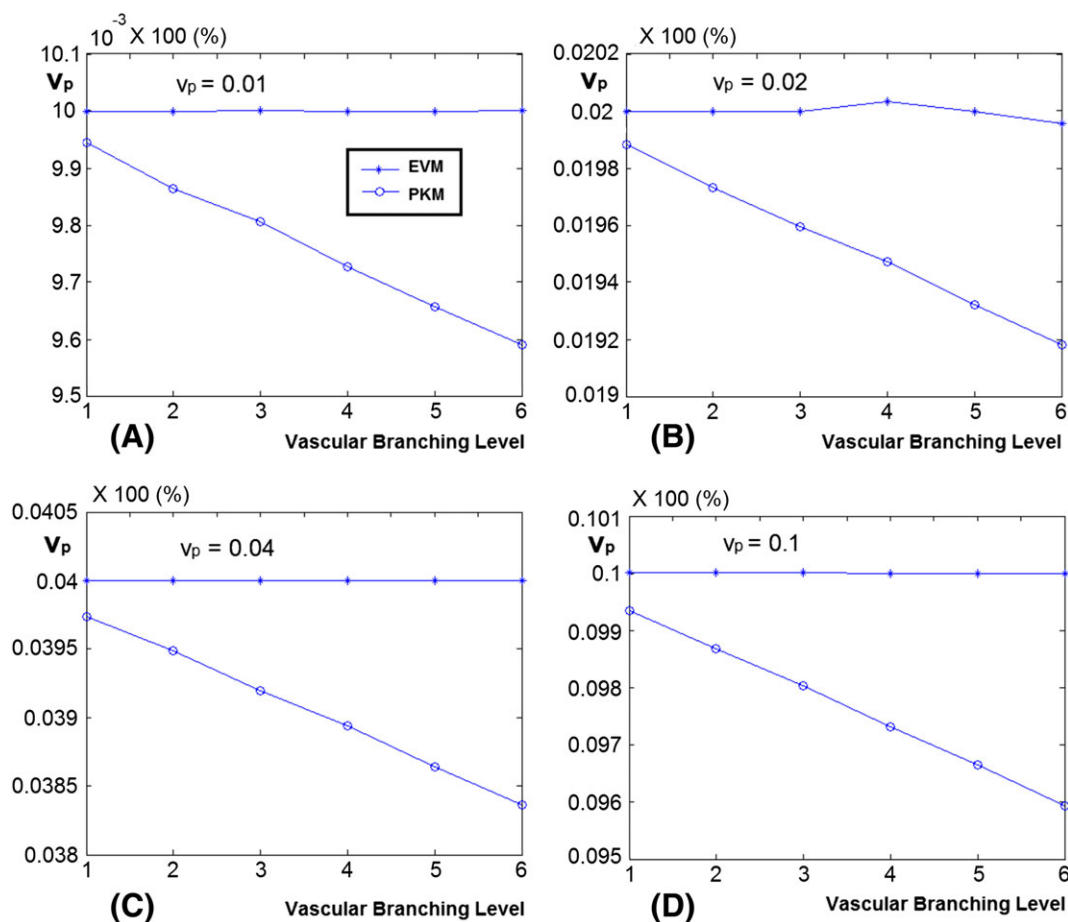

FIGURE 6 A, The v_p values estimated by solving the pharmacokinetic model equation using the global AIF and local AIF estimated with the vascular model. When the model corrected local AIF is used, the estimated value of v_p is much closer to the nominal value compared with using the global AIF, which leads to underestimation of v_p. B-D, The estimated values of v_p for simulating a fractional plasma volume of 0.02, 0.04 and 0.1

is the possibility of existence of branches having higher number of bifurcations, in such events, $n = 6$ would be selected as the best configuration of the function. One of the drawbacks of this method is the relatively long processing time due to the 18 configurations of the model that are being fit to the data. One solution to solving this would be to use adaptive models for this part of the methods.

In the simulation study, although the full range of parameters was not considered, the results show that when the local AIF is used, the estimated parameters are less biased compared with the case of using the global AIF. Although in this study the transfer function based on the extended model was used to simulate the tissue concentration signals and transform the AIF, based on our model we expect the simulated signals to be a reasonable estimation of the signals in real tissue. The accuracy of the results shows the reliability of this model for estimating the permeability parameters by decomposing the tissue concentration signal into the intravascular and extravascular components, which is the main advantage compared with using the global AIF. Comparing these simulation results with the results obtained from processing the DCE-MRI data from the tumor patients confirms that

when the global AIF is used for solving the pharmacokinetic equation, the permeability parameters estimated in the tumor area are overestimated or underestimated with the same trend as the simulation study. These results confirm the findings by Fluckiger et al when they used a local AIF for measuring the permeability parameters.[16]

One issue with any suggested model in DCE studies is clinically validating the estimated parameters in the human brain.[28] Although there have been attempts to address this issue by developing phantoms to simulate perfusion, most of these systems fail to establish and accurately replicate physiologically relevant capillary permeability and exchange performance. One approach to solving this problem has been using concepts of physics and transport phenomena for better understanding of CA kinetics. In one approach, Peladeau-Pigeon and Coolens[28] used the results of a computational fluid dynamics simulation and DCE-CT data obtained from a flow phantom to test Tofts'[29] enhanced model and Fick's principle.[30] The phantom used in this study contained a single tube. Our simulation is a similar approach for simulating such a physical model; however, effects of dispersion due to vascular branching and flow have also been incorporated in
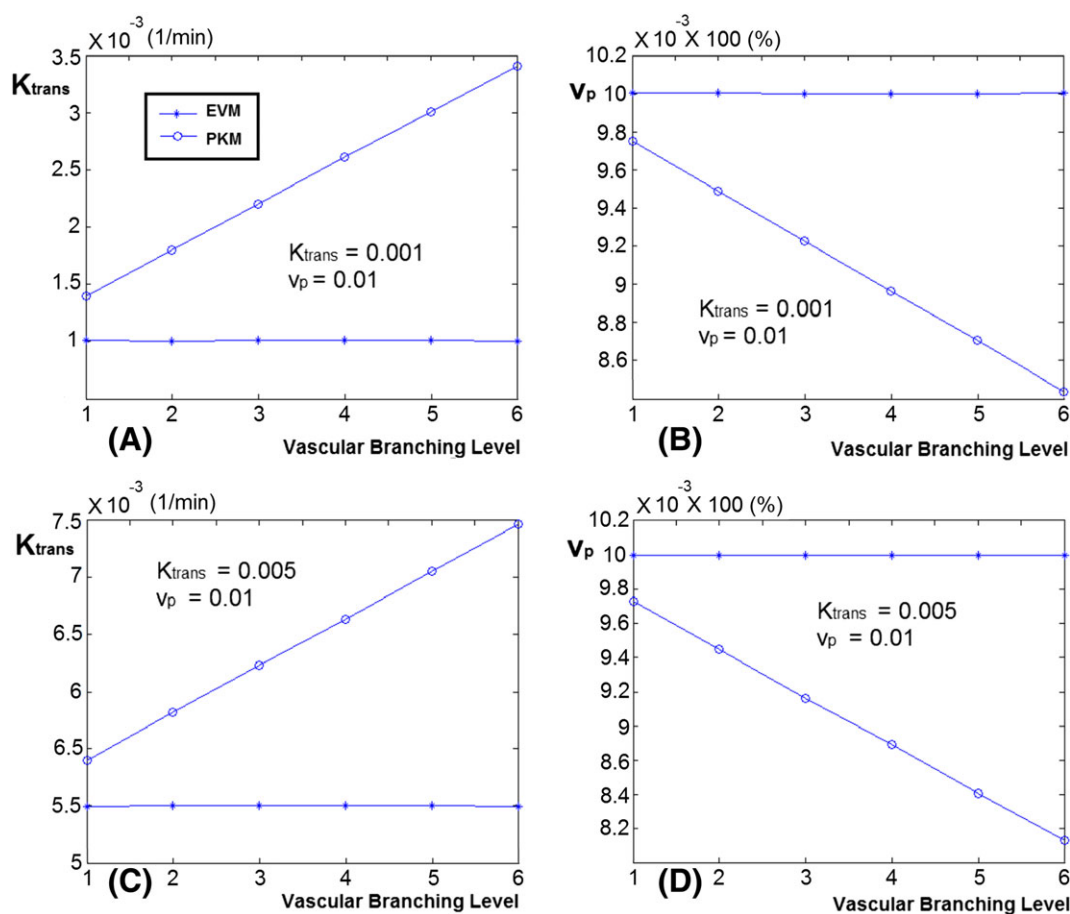

FIGURE 7 Estimated values of K^{trans} and v_p calculated by solving the pharmacokinetic model using the global AIF and the local AIF estimated with the vascular model for simulated signals. These signals were created assuming that they are sampled from six different levels of the vascular tree. Also, leakage was added to the vessels based on the second configuration of the pharmacokinetic model, where only K^{trans} and v_p exist in the equation. A,B, $v_p = 0.01$ and $K^{trans} = 0.001$/min; C,D, $v_p = 0.01$ and $K^{trans} = 0.005$/min. As seen here, in both configurations, the K^{trans} values found using the global AIF are overestimated at all branching levels, and as the vascular levels increase this value increases as well. In the case of $K^{trans} = 0.001$ the overestimation is about nine times the nominal value, and in the case of $K^{trans} = 0.005$ it is about three times. In contrast, when using the vascular model, the estimated value of K^{trans} is equal to the nominal value. In the case of v_p, similar to the case of the first configuration of the pharmacokinetic model, in the case of using the global AIF the fractional plasma volume is underestimated from the first level and by the sixth level is underestimated by about 80% of the nominal value. In the case of using the local AIF the estimated value of v_p is always accurate

our model. Although validation of the results for *in vivo* human data is not possible, in the next step, to further investigate the accuracy of these results, these methods will be applied to DCE-T1 images of animals. Assessment of the accuracy of either method for estimating the permeability parameters can be investigated using methods such as histology or autoradiography; however, the results of the simulation study lean towards accuracy of the values found by the extended model.

In conclusion, we have introduced a model of the brain vasculature that describes the flow of blood in the brain vessels and also leakage of the CA to the EES. This model can be used to estimate the local AIF in

brain areas with vessels with or without leakage of the CA. Our simulations show that using the local AIF estimated by this model to solve the SM can give less biased estimations of the permeability parameters compared with using the global AIF. Using this model on DCE-MR images of cerebral tumors to estimate the permeability parameters yielded similar results as the simulations. One application of this model may be simultaneous estimation of the intravascular component of the CA concentration signal and the permeability parameters in areas with vascular extravasation. To validate the accuracy of the method for estimating the permeability parameters, it should be applied to DCE images of animals. Further additions to this model can include effects
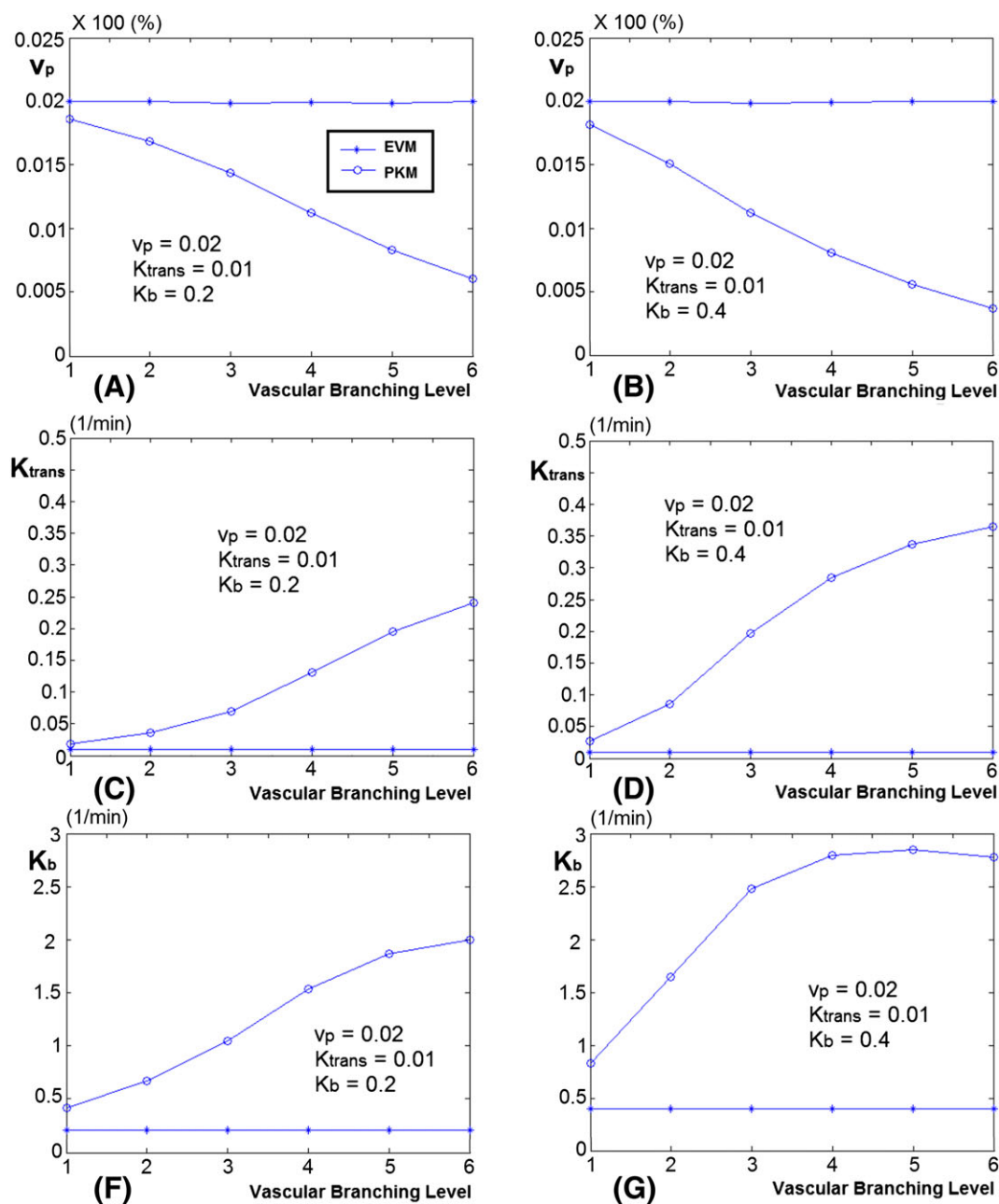

FIGURE 8 Estimated values of v_p, K^{trans} and K_b, using the pharmacokinetic model and global AIF versus the local AIF corrected by the vascular model. The curves on the left represent the case where $K_b = 0.2$ and the curves on the right represent $K_b = 0.4$. In both cases $K^{trans} = 0.01$ and $v_p = 0.02$. As seen in both cases, the value of v_p estimated using the vascular model is almost the same as the nominal value. The estimated values of K^{trans} and K_b are close to the nominal value, and even though at some of the branching levels they deviate from this value this is much less than in the case of the estimates made using the global AIF. In this case, the value of K^{trans} can be overestimated as much as 20-fold and K_b is as high as six times the nominal value

of the capillaries on dispersion of the AIF so that this model can be used for more accurate estimation of perfusion parameters in DCE-CT and DSC-MR images.

ACKNOWLEDGEMENT

CONFLICT OF INTEREST

The authors declare that they have no conflicts of interest in the research.

REFERENCES

1. Nejad-Davarani SP, Bagher-Ebadian JR, et al. A parametric model of the brain vascular system for estimation of the arterial input function (AIF) at the tissue level. *NMR in Biomedicine*. 2017;e3695. https://doi.org/10.1002/nbm.3695

2. Gall P, Guether M, Kiselev V. Model of blood transport couples delay and dispersion and predicts ASL bolus measurements. *Proc Int Soc Magn Reson Med*. 2010;18:1736.

3. Kellner E, Gall P, Gunther M, et al. Blood tracer kinetics in the arterial tree. *PLoS One*. 2014;9(10):e109230.

4. Gall P, Petersen ET, Golay X, Kiselev V. Delay and dispersion in DSC perfusion derived from a vascular tree model predicts ASL measurements. *Proc Int Soc Magn Reson Med*. 2008;16:627.

5. Gall P, Kiselev V. On the form of the residue function for brain tissue. *Proc Int Soc Magn Reson Med*. 2010;18:1795.

6. Sourbron S, Ingrisch M, Siefert A, Reiser M, Herrmann K. Quantification of cerebral blood flow, cerebral blood volume, and blood–brain-barrier leakage with DCE-MRI. *Magn Reson Med*. 2009;62(1):205–217.

7. Guzman-de-Villoria JA, Fernandez-Garcia P, Mateos-Perez JM, Desco M. Estudio de la perfusion cerebral mediante tecnicas de susceptibilidad magnetica: tecnica y aplicaciones [Studying cerebral perfusion using magnetic susceptibility techniques: technique and applications]. *Radiologia*. 2012;54(3):208–220.

8. Chan AA, Nelson SJ. Simplified gamma-variate fitting of perfusion curves. In: *IEEE International Symposium on Biomedical Imaging (ISBI)*, Arlington, VA, USA. 2004; 1067–1070.

9. Nestorov I. Whole-body physiologically based pharmacokinetic models. *Expert Opin Drug Metab Toxicol*. 2007;3(2):235–249.

10. Bagher-Ebadian H, Jain R, Nejad-Davarani SP, et al. Model selection for DCE-T1 studies in glioblastoma. *Magn Reson Med*. 2012;68(1):241–251.

11. Tofts PS, Brix G, Buckley DL, et al. Estimating kinetic parameters from dynamic contrast-enhanced T_1-weighted MRI of a diffusable tracer: standardized quantities and symbols. *J Magn Reson Imaging*. 1999;10(3):223–232.

12. Calamante F. Arterial input function in perfusion MRI: a comprehensive review. *Prog Nucl Magn Reson Spectrosc*. 2013;74:1–32.

13. Sourbron SP, Buckley DL. Classic models for dynamic contrast-enhanced MRI. *NMR Biomed*. 2013;26(8):1004–1027.

14. Calamante F, Gadian DG, Connelly A. Delay and dispersion effects in dynamic susceptibility contrast MRI: simulations using singular value decomposition. *Magn Reson Med*. 2000;44(3):466–473.

15. Lee JJ, Bretthorst GL, Derdeyn CP, et al. Dynamic susceptibility contrast MRI with localized arterial input functions. *Magn Reson Med*. 2010 May;63(5):1305–1314.

16. Fluckiger JU, Schabel MC, DiBella EV. Toward local arterial input functions in dynamic contrast-enhanced MRI. *J Magn Reson Imaging*. 2010;32(4):924–934.

17. Yankeelov TE, Luci JJ, Lepage M, et al. Quantitative pharmacokinetic analysis of DCE-MRI data without an arterial input function: a reference region model. *Magn Reson Imaging*. 2005;23(4):519–529.

18. Nejad Davarani SP, Bagher-Ebadian H, Ewing JR, Chopp M, Noll D, Jiang Q, eds. Analytical model of the brain vascular system for estimation of the arterial input function (AIF) at the tissue level. Presented at: WorldComp'12; July 16–19, 2012; Las Vegas, NV.

19. Wright SN, Kochunov P, Mut F, et al. Digital reconstruction and morphometric analysis of human brain arterial vasculature from magnetic resonance angiography. *Neuroimage*. 2013;82C:170–181.

20. Lagarias JC, Reeds JA, Wright MH, Wright PE. Convergence properties of the Nelder–Mead simplex method in low dimensions. *SIAM J Optim*. 1998;9:36.

21. Posada D, Buckley TR. Model selection and model averaging in phylogenetics: advantages of Akaike information criterion and Bayesian approaches over likelihood ratio tests. *Syst Biol*. 2004;53(5):793–808.

22. O'Connor JP, Tofts PS, Miles KA, Parkes LM, Thompson G, Jackson A. Dynamic contrast-enhanced imaging techniques: CT and MRI. *Br J Radiol*. 2011;84:(Spec No. 2):S112–S120.

23. Ewing JR, Bagher-Ebadian H. Model selection in measures of vascular parameters using dynamic contrast-enhanced MRI: experimental and clinical applications. *NMR Biomed*. 2013;26(8):1028–1041.

24. Deoni SC, Peters TM, Rutt BK. High-resolution T_1 and T_2 mapping of the brain in a clinically acceptable time with DESPOT1 and DESPOT2. *Magn Reson Med*. 2005;53(1):237–241.

25. Strich G, Hagan PL, Gerber KH, Slutsky RA. Tissue distribution and magnetic resonance spin lattice relaxation effects of gadolinium-DTPA. *Radiology*. 1985;154(3):723–726.

26. Bagher-Ebadian H, Paudyal R, Nagaraja TN, Croxen RL, Fenstermacher JD, Ewing JR. MRI estimation of gadolinium and albumin effects on water proton. *Neuroimage*. 2011;54(Suppl. 1):S176–S179.

27. Lomax RG. *An Introduction to Statistical Concepts*. 2nd ed. Mahwah, NJ: Erlbaum; 2007.

28. Peladeau-Pigeon M, Coolens C. Computational fluid dynamics modelling of perfusion measurements in dynamic contrast-enhanced computed tomography: development, validation and clinical applications. *Phys Med Biol*. 2013;58(17):6111–6131.

29. Sourbron SP, Buckley DL. On the scope and interpretation of the Tofts models for DCE-MRI. *Magn Reson Med*. 2011;66(3):735–745.

30. Truskey GA, Yuan F, Katz DF. *Transport Phenomena in Biological Systems*. 2nd ed. Pearson Prentice Hall: Upper Saddle River, NJ; 2009.